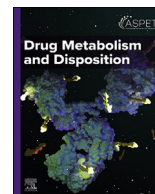




Drug Metabolism and Disposition



journal homepage: www.dmd.aspetjournals.org



SPECIAL SECTION: SEX AND HORMONAL INFLUENCES ON DRUG METABOLISM AND DISPOSITION, AND RELATED STUDIES—ARTICLE

Impact of the loss of *slc43a3* on 6-mercaptopurine absorption and tissue distribution in mice



Aaron L. Sayler, Hannah Dean , James R. Hammond* 

Department of Pharmacology, University of Alberta, Edmonton, Alberta, Canada

ARTICLE INFO

Article history:

Received 7 January 2025

Accepted 13 February 2025

Available online 3 March 2025

Key words:

chemotherapy
mouse model
nucleobase transporter
pharmacokinetics
purine analogs


ABSTRACT

6-Mercaptopurine (6-MP) is a nucleobase analog used in the therapy of acute lymphoblastic leukemia and inflammatory bowel disease. It is associated with numerous side effects including myelotoxicity, hepatotoxicity, and gastrointestinal complications, which can lead to patient adherence issues or discontinuation of treatment. This is further complicated by the wide variability in plasma levels of 6-MP and the therapeutic response to a standard dose. Although a number of enzyme polymorphisms have been linked to therapeutic response, it is unclear what factors underlie the variability in plasma levels. We have established that *SLC43A3*-encoded equilibrative nucleobase transporter 1 mediates the transport of 6-MP into cells in both mice and humans. To determine whether this transporter is critical for 6-MP absorption and biodistribution, we examined the effect of the genetic deletion of *slc43a3* in mice on the absorption and tissue distribution of orally administered 6-MP. A high-performance liquid chromatography method was developed to measure tissue levels of 6-MP and its key metabolites, 6-methylmercaptopurine, 6-thiourate, and 6-thioguanine nucleotides. The results of this study show that loss of *slc43a3* dramatically reduces the absorption of 6-MP from the gastrointestinal tract and attenuates the levels achieved in peripheral tissues. Furthermore, the loss of *slc43a3* decreases the tissue:blood concentration ratios of 6-MP and its metabolites, particularly in those tissues that show high levels of expression of *slc43a3*, such as the heart and lungs. Therefore, it is possible that differences in *SLC43A3* expression in humans may contribute to the variability seen in 6-MP plasma levels and therapeutic response.

Significance Statement: The loss of *slc43a3* in mice dramatically reduces the absorption and the bio-distribution of the chemotherapeutic drug 6-mercaptopurine. These data suggest that variations in *SLC43A3* expression in humans may contribute to the variability in plasma levels that have been reported when using this drug therapeutically.

© 2025 The Author(s). Published by Elsevier Inc. on behalf of American Society for Pharmacology and Experimental Therapeutics. This is an open access article under the CC BY-NC-ND license (<http://creativecommons.org/licenses/by-nc-nd/4.0/>).

* **Address correspondence to:** Dr James R. Hammond, Department of Pharmacology, University of Alberta, 9-70 Medical Sciences Building, Edmonton, Alberta T6G2H7, Canada. E-mail: james.hammond@ualberta.ca

 This article has supplemental material available at dmd.aspetjournals.org.

This work was previously presented at national conferences as follows: Sayler A, Dean H, Kim CS, Hammond JR (2023) Impact of loss of *SLC43A3* on the biodistribution and metabolism of 6-mercaptopurine in mice. *7th Canadian Cancer Research Conference*; 2023; Halifax, Canada.

Sayler AL, Dean H, Hammond JR (2024) Loss of the *slc43a3*-encoded equilibrative nucleobase transporter 1 in mice reduces the gastrointestinal absorption of 6-mercaptopurine. *Annual Meeting of the Canadian Society of Pharmacology and Therapeutics*; 2024; Ottawa, Canada.

1. Introduction

6-Mercaptopurine (6-MP) and its prodrug azathioprine (AZA) are used extensively in the therapy of pediatric acute lymphoblastic leukemia (Estlin, 2001; Toksvang et al, 2022) and inflammatory bowel diseases (IBD; Nielsen et al, 2001; Dubinsky, 2004). Although effective in these therapies, their use is associated with a number of adverse effects such as myelosuppression and hepatotoxicity. Other minor side effects include nausea, vomiting, and loss of appetite. The impact of these adverse effects is exacerbated by the wide range of plasma concentrations of 6-MP achieved with a standard dose (Lonnerholm et al, 1986; Endresen et al, 1990), which can lead to insufficient therapy or an increase in adverse effects. These issues can lead to problems with adherence to the dosing schedule,

<https://doi.org/10.1016/j.dmd.2025.100054>

0090-9556/© 2025 The Author(s). Published by Elsevier Inc. on behalf of American Society for Pharmacology and Experimental Therapeutics. This is an open access article under the CC BY-NC-ND license (<http://creativecommons.org/licenses/by-nc-nd/4.0/>).

particularly in a pediatric patient population, which is associated with poorer therapeutic outcomes and increased risk of relapse (Gupta and Bhatia, 2017). This interpatient variability has been attributed to a combination of environmental and genetic factors (Lafolie et al, 1989). A number of polymorphisms in key enzymes in the 6-MP metabolic pathway, such as thiopurine methyltransferase (TPMT) (McLeod et al, 2000; Abaji and Krajcinovic, 2017), inosine triphosphate pyrophosphatase (Barba et al, 2022), and nudix hydrolase 15 (Du et al, 2024), have been identified and tied to variability in 6-MP effects. However, mutations in these enzymes neither explain all of the variability in response observed nor do they adequately explain why 6-MP plasma concentrations vary so widely.

Drug transporters are increasingly recognized as a major factor in the absorption and biodistribution of many drugs (Yuasa et al, 2020; Galetin et al, 2024). Until recently, the transporters involved in the flux of 6-MP across cell membranes were poorly defined. The equilibrative nucleoside transporters ENT1 and ENT2 can transport 6-MP with K_m values in the millimolar range (Nagai et al, 2007; Yao et al, 2011), 3 orders of magnitude above the therapeutic plasma concentrations of 6-MP (low micromolar; Endresen et al, 1990; Kato et al, 1991). Therefore, although the ENTs may have some impact on 6-MP pharmacokinetics, they would likely be minor contributors. In rodents, SNBT1, encoded by *slc23a4*, was identified as a sodium-dependent concentrative transporter for nucleobases such as 6-MP (Yamamoto et al, 2010). However, the human *SLC23A4* has been shown to be a pseudogene that lacks 3 TM-encoding exons and does not produce a functional nucleobase transporter protein (Yamamoto et al, 2010).

The most likely candidate for the transporter mediating the membrane flux of 6-MP is ENBT1, encoded by the gene *SLC43A3*. Our laboratory has established that this facilitated diffusion system transports 6-MP into a variety of murine and human cells in vitro at concentrations in the therapeutic range (Ruel et al, 2019, 2022; Kim et al, 2024). We have also confirmed that the murine ENBT1 transports 6-MP with the same kinetic parameters as the human ortholog (Kim et al, 2024). This supports the clinical relevance of using a mouse model for research into the role of ENBT1 in an in vivo setting. To this end, we report herein on the development of a *slc43a3*-null mouse model and its use to assess the role of *slc43a3*-encoded ENBT1 in the absorption and biodistribution of orally administered 6-MP. We hypothesized that the loss of ENBT1 would disrupt 6-MP absorption from the gastrointestinal (GI) lumen into circulation and subsequently its distribution to secondary pharmacokinetic compartments.

2. Materials and methods

2.1. Materials

All primers were ordered through Integrated DNA Technologies. The 100-bp DNA Ladder was obtained from FroggaBio Inc. Agarose, Oligo(dT)_{12–18} primer, HEPES, PowerTrack SYBR Green, TRIzol Reagent, SuperScript III Reverse Transcriptase, 6-methylmercaptapurine (6-MMP), and H₃PO₄ were obtained from Thermo Fisher Scientific. KAPA Biosystem Genotyping Kit, 6-MP, 6-thioguanine (6-TG), dithiothreitol, triethylamine, methanol, and AZA were purchased from Sigma-Aldrich; 6-thiourate (6-TU) was purchased from Toronto Research Chemicals.

2.2. Generation of the *slc43a3*-null mice

The generation of the *slc43a3*-null C57BL/6J mice was outsourced to Cyagen Biomodels. The *slc43a3* gene (NCBI Reference Sequence: NM_021398.3; Ensemble: ENSMUSG00000027074) is located on mouse chromosome 2. Thirteen exons were identified,

with the ATG start codon in exon 2 and the TAG stop codon in exon 13 (Transcript *slc43a3*-201: ENSMUST00000090726). Thus, exons 3–12 on chromosome 2 were targeted via coinjection of Cas-9 and gRNA into fertilized eggs for the production of *slc43a3*-null mice. The gRNA target sequences were as follows: gRNA-A1 (matching forward strand of gene): CAAAGTTGTCAAGGTAGAGGGG; gRNA-A2 (matching forward strand of gene): AATATGTGTTACTCCAGAATAGG; gRNA-B1 (matching reverse strand of gene): AAAGTCCCCCTCTAAAC-CAGG; gRNA-B2 (matching forward strand of gene): CTGGGGCTTCCTAAGGTCGAGG. The size of the effective deletion is 18,660 bp while adding a 96 bp region to positively identify alleles with the *slc43a3* deletion.

A breeding colony was established at Health Sciences Laboratory Animal Services Facility, University of Alberta, via the mating of heterozygous (HET; *slc43a3*^{+/-}) mice for the generation of homozygous wild-type (WT; *slc43a3*^{+/+}) and *slc43a3*-knockout (KO; *slc43a3*^{-/-}) mice. Pups were ear-notched for identification before reaching 3 weeks of age. All animal work was conducted according to the Canadian Council on Animal Care standards using protocols (AUP00002022) approved by the Animal Care Committee of the Faculty of Medicine & Dentistry, University of Alberta.

Tissue samples (~1 µg) from the ear notch were used for genotyping. DNA was extracted and processed using the KAPA Mouse Genotyping kit according to the manufacturer's protocol. Template DNA obtained from the KAPA Express Extract Protocol underwent the following PCR cycling protocol in the presence of the primers shown in Supplemental Table 1: 94 °C for 3 minutes, followed by 35–40 cycles of 30 seconds at 94 °C, 35 seconds at 60 °C, and 35 seconds at 72 °C, followed by an additional extension time of 5 minutes at 72 °C. The resulting PCR products were loaded onto a 1.5% agarose gel and resolved at 80 V for 40 minutes. The resolved bands were visualized via chemiluminescence on an Amersham Imager 680 (GE Healthcare). *Slc43a3*-KO homozygotes were identified by the presence of 1 band of 365 bp. Heterozygotes were determined by the presence of 2 bands at 365 and 536 bp. WT mice were identified by the presence of 1 band at 536 bp (Supplemental Fig. 1).

2.3. Semiquantitative polymerase chain reaction (qPCR)

Mice were euthanized via carbon dioxide overdose in the Health Sciences Laboratory Animal Services Facility according to the protocols approved by the Animal Care Committee of the Faculty of Medicine & Dentistry, University of Alberta. Dissections were performed swiftly to isolate the heart, lungs, liver, kidneys, duodenum, and jejunum. Tissues were immediately flash-frozen in liquid nitrogen following their isolation and stored at –80 °C until use. For RNA extractions, frozen tissues were crushed using a mortar and pestle before suspension and homogenization in TRIzol (Applied Biosystems, item #AM9736) at a concentration of 1 mL/100 mg of tissue, and total RNA was isolated according to the TRIzol Reagent Solution provider (Applied Biosystems) protocol. Total RNA concentration and purity were determined using a Nanodrop 2000 spectrophotometer (Life Technologies Inc). For cDNA synthesis, 1 µg of total RNA was reverse transcribed to complementary DNA (cDNA) using Oligo(dT)_{12–18} primer and Superscript III Reverse Transcriptase. Semiquantitative PCR was then conducted using this cDNA and the primer sets shown in Supplemental Table 2 to assess the relative expression of a range of genes encoding enzymes and transporters involved in 6-MP transport and metabolism. PCR conditions were 2 minutes at 95 °C, followed by 40 cycles of both 15 seconds at 95 °C and 60 seconds at 60 °C, with a final melt curve analysis, using PowerTrack SYBR Green detection on a Roche Light Cycler 480 System (Cardiovascular Research Centre). Ct values were normalized to the geometric mean of the

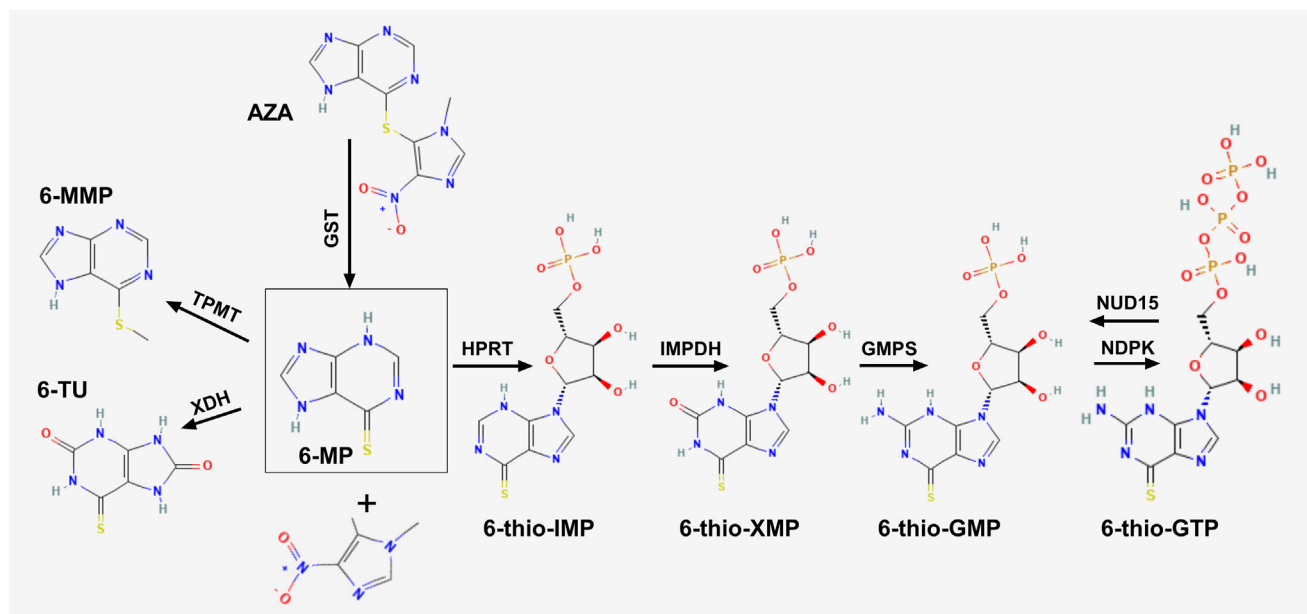


Fig. 1. 6-MP metabolism. Diagram showing the metabolic pathway and the 6-MP metabolites considered in this study. Enzymes, GST, glutathione S-transferase, TPMT, thiopurine methyltransferase, XDH, xanthine dehydrogenase, HPRT, hypoxanthine-guanine phosphoribosyltransferase, IMPDH, inosine 5'-monophosphate dehydrogenase, GMPS, guanosine monophosphate synthase, NDPK, nucleoside-diphosphate kinase, NUD15, nudix hydrolase 15. Molecular structures obtained from PubChem (<https://pubchem.ncbi.nlm.nih.gov>).

reference genes *gapdh* and *actb* to obtain ΔC_t values for comparative statistical analyses.

2.4. Oral gavage

Mice were used for experiments at 10–12 weeks of age. This is the average age at which a mouse is generally considered a sexually mature adult (Dutta and Sengupta, 2016). Total body mass of male and female WT and KO mice was measured, and the mice were then administered 75 mg/kg 6-MP or 156 mg/kg AZA dissolved in 0.1 M NaOH via oral gavage. This dose of 6-MP is 37.5× the maximum dose given to humans, as per allometric scaling recommendations for rodents (Nair and Jacob, 2016). AZA is 55% of 6-MP by molecular weight, and 88% of AZA is converted to 6-MP, such that a conversion factor of 2.08 must be taken into account when calculating equivalent doses of 6-MP and AZA. The distance from the oral cavity to the end of the xiphoid process was measured using a sterile plastic 20-gauge × 38 mm gavage cannula (Instech). The cannula was placed on the right lateral side of the oral cavity ensuring no incisor piercing of the plastic cannula tube. It was then slid down and rotated slightly to bypass the epiglottis to enter the esophagus. The cannula is visibly swallowed, eliminating any resistance in cannula movement and allowing entry of the cannula tip into the stomach. The content of the loaded gavage tube (6-MP or AZA solution) was injected into the stomach over a span of several seconds so as not to cause the mouse to regurgitate or aspirate the solution, ensuring full delivery of the entire volume of 200 μ L.

2.5. Tissue/organ harvesting

6-MP and metabolite content was assessed in organs, blood, and feces at various time points (30, 90, 180, and 270 minutes) following the administration of 6-MP. These incubation times were selected based on the reported half-life of 6-MP of about 1.5 hours in both humans (Lonnerholm et al, 1986) and mice (Kurowski and Iven, 1991), although in humans, it has been reported to range from 0.7 to 2.8 hours (Lonnerholm et al, 1986). The incubation times after

treatment with 6-MP covers this range of half-lives to nominally capture the absorption phase, peak, and elimination phase of the pharmacokinetic profile for 6-MP.

At the specified times after drug administration, mice were transferred to a sealed single-mouse induction chamber. The chamber was delivered oxygen for 4–5 breaths for preoxygenation, then filled with 3%–5% (vol/vol) isoflurane (Piramal Healthcare Ltd), in a stepwise manner to provide smooth induction, until a surgical plane of anesthesia was achieved. Mice were then transferred to a surgery platform, and surgical anesthesia was maintained with 1%–3% isoflurane using a nose cone and Bain circuit. Reflex assessment and responses to stimuli were continuously monitored to ensure the maintenance of anesthesia.

Blood samples were acquired via cardiac puncture while in deep surgical anesthesia to ensure blood pressure was sufficient to allow for adequate collection. The average circulating blood volume of a 25-g young adult mouse is 1.4 mL. If insufficient blood was obtained by cardiac puncture, the chest cavity was immediately opened, and the needle was placed directly into the heart for blood collection. The heart, lungs, liver, kidneys, spleen, and small intestine were then immediately removed. The intestines were cleared of fecal content (retained for analysis) and cut into their individual components (duodenum, jejunum, and ileum) for collection using estimated lengths from previous publications (Casteleyn et al, 2010). All organs and tissues collected were pat-dried, weighed, and flash-frozen using liquid nitrogen and stored at -20°C .

2.6. High-performance liquid chromatography sample preparation

All tissues, organs, and feces harvested from 6-MP-treated mice were kept submerged in liquid nitrogen until pulverization under pestle and mortar. The homogenized sample was then subjected to an extraction procedure based on that of Dervieux and colleagues (Dervieux and Boulieu, 1998). The samples were mixed with 10 μ L of dithiothreitol dissolved in 70% perchloric acid to protect the thio-containing components from oxidation. Contents were vortexed for 30 seconds in a 2-mL Eppendorf tube (Sarstedt, Canada), followed

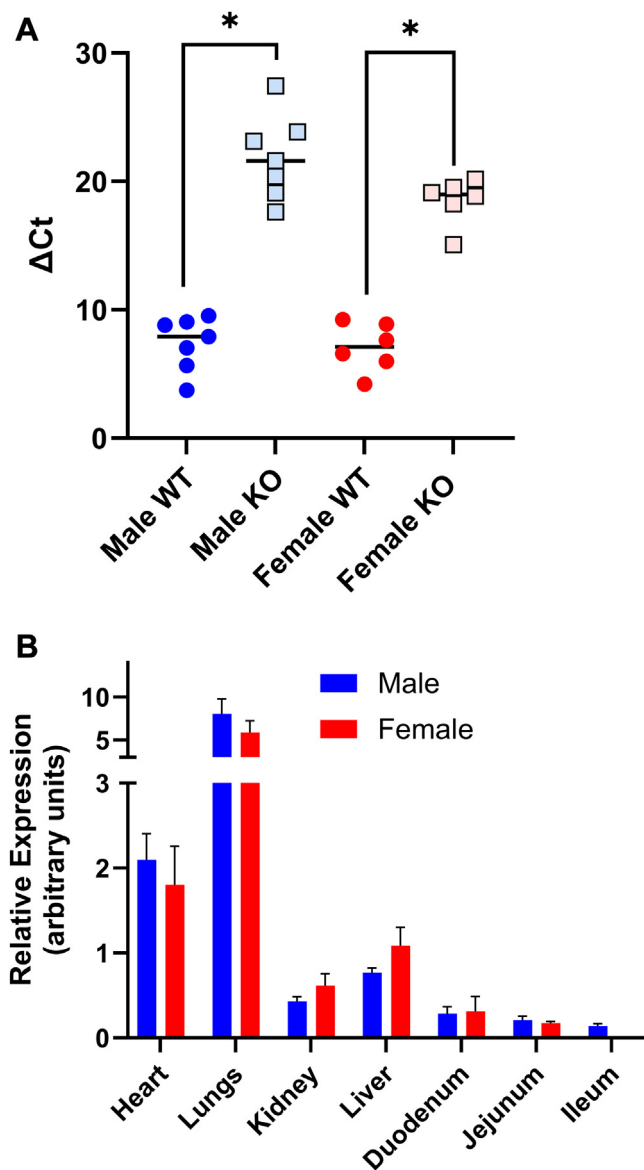


Fig. 2. *Slc43a3* expression. (A) Comparison of *slc43a3* transcript levels in male and female WT and KO mice. Each point is the average ΔC_t for each of the tissues examined. Significant differences between WT and KO mice are denoted with an asterisk (two-way ANOVA with the Tukey post-test for multiple comparisons, $P < .05$). (B) Comparison of expression of *slc43a3* in male and female WT mice across tissue types. Transcript levels were determined by qPCR relative to the geometric mean of *gapdh* and *actb* (ΔC_t) and converted to relative expression using the formula $2^{-\Delta C_t} \times 100$. Each bar represents the mean \pm SEM from 4 to 5 independent tissues. There were no significant differences between males and females ($P < .05$, two-way ANOVA corrected for multiple comparisons using the Tukey method).

by heating for 45 minutes at 100 °C to hydrolyze thiopurine nucleotides into their corresponding bases (Dervieux and Boulieu, 1998). After cooling, the samples were centrifuged at 15,000 rcf for 10 minutes to separate the liquid from the debris pellet. The supernatant was collected, leaving the solid debris pellet behind, and stored at -20 °C pending further processing. Removal of lipid contaminants from these samples was based on the Folch method (Folch et al, 1957). To create a biphasic system in which the lipids would be restricted to the organic phase, a 2:1 (v/v) solvent mixture of chloroform/methanol was added to each sample in a 2-mL Eppendorf tube. This was then centrifuged for 10 seconds at $\sim 2000g$ to separate into an organic phase containing lipid

contaminants and an aqueous phase holding 6-MP and its metabolites. The aqueous extracts were immediately dried under a stream of nitrogen to ensure the remaining solvents and chloroform were removed, and then stored at -20 °C.

2.7. High-performance liquid chromatography analysis

6-MP is metabolized intracellularly to 6-TU by xanthine dehydrogenase (XDH), 6-MMP by TPMT, or ultimately to 6-TGN by the sequential actions of hypoxanthine-guanine phosphoribosyltransferase, inosine 5'-monophosphate dehydrogenase, and guanosine monophosphate synthetase (GMPS) (Fig. 1). To determine how the loss of *slc43a3* impacted the biodistribution of 6-MP and these primary metabolites, an high-performance liquid chromatography (HPLC) method was optimized for the simultaneous measurement of these compounds in the various tissues. HPLC was conducted using an Agilent 1100 instrument equipped with a FCV-10AL low-pressure solvent selector valve with a quaternary pump and Alltech ELSD2000 Evaporative Light-Scattering Detector via diode array detection, using a modified version of the method of Oliveira and colleagues (Oliveira et al, 2004). The separation was carried out using an Infinity Lab Poroshell 120 SB-C18 column with a 4- μm particle diameter, a 21.2-mm inner diameter, and 150 mm length (Agilent Technologies). The HPLC instrument utilized an auto-injector set to inject 10 μL volumes from each sample tested. Elution was with a dual mobile phase gradient at a flow rate of 0.7 mL/minute. Mobile phases were made immediately prior to starting a run and had a shelf life of approximately 1 week at room temperature. Mobile phase A was composed of water purified through a Milli-Q Plus system with 1.3% triethylamine acidified to a pH of 3.2 with 0.1 M phosphoric acid. Mobile phase B was composed of water:methanol (50:50, v/v) with 1.3% triethylamine acidified to a pH of 3.2 with 0.1 M phosphoric acid. Mobile phase A started at 100% with mobile phase B introduced at 4% per minute for 10 minutes to a total of 40%. Mobile phase B was then returned to 0% for the final 5 minutes (100% mobile phase A), for a total run time of 15 minutes at 23.5 °C. The column effluent was monitored simultaneously at 303 nm for 6-MMP, 322 nm for 6-MP, and 342 nm for 6-TG and 6-TU (Oliveira et al, 2004; Adam de Beaumais et al, 2022). The elution times for each analyte were 5.7, 5.9, 6.5, and 8.0 minutes for 6-TG, 6-TU, 6-MP, and 6-MMP, respectively. After each set of HPLC runs, the column was washed with acetonitrile:water (50:50, v/v) and stored. The guard column was replaced after approximately 300 injections. A representative chromatogram is shown in Supplemental Fig. 2.

2.8. HPLC standard curves

The standard curves for detection of 6-MP, 6-TG, 6-TU, and 6-MMP were constructed using a minimum of 6 concentrations of each analyte prepared in an organ matrix to resemble the experimental samples. The organ matrix consisted of a blended filtrate of all the tissues assessed after they were homogenized, hydrolyzed, and filtered. The concentration ranges used were designed to cover the range expected from the experimental sample analyses. Three technical replicates were completed for each concentration of the analytes of interest and the area under the curve (Agilent ChemStation software) averaged for the peaks representing each analyte concentration to build the profiles shown in Supplemental Fig. 3. Note that the standard curves were all linear over the concentration range used. These standard curves were then used to back-calculate the amount of each analyte per sample based on peak area. During each HPLC sample analysis run, interassay standards were analyzed using 1230 pmol/10 μL 6-TG, 1500 pmol/10 μL 6-TU, 1200 pmol/10 μL 6-MP, and 24,000 pmol/10 μL 6-MMP

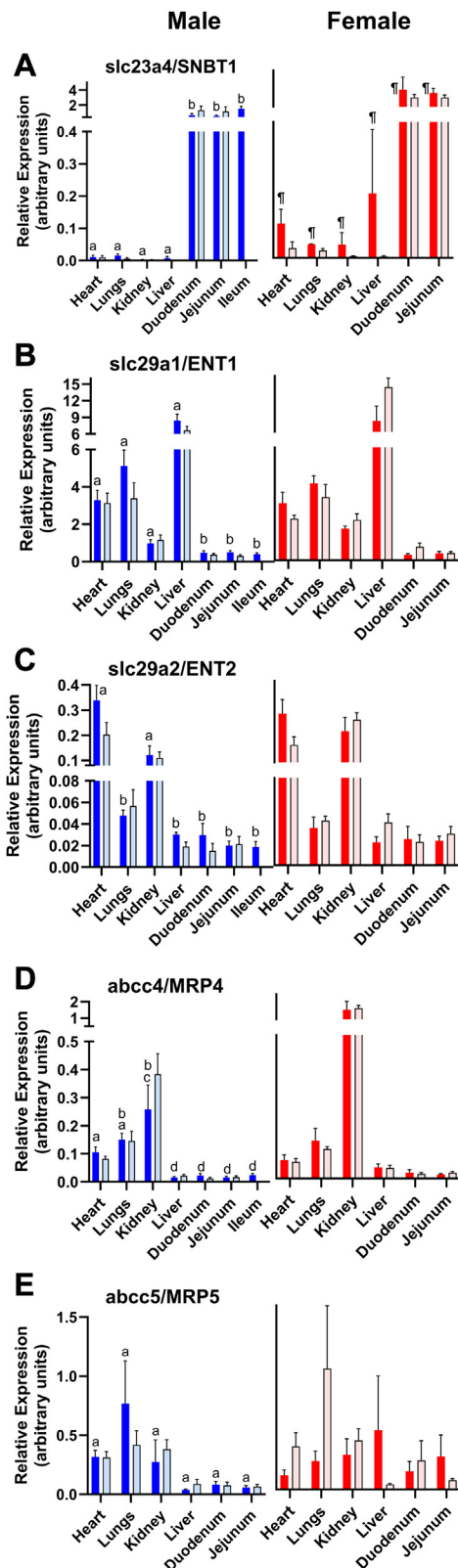


Fig. 3. Expression of genes in WT and KO mice encoding for membrane transporters that potentially transport 6-MP and its metabolites. Transcript levels were determined by qPCR relative to the geometric mean of *gapdh* and *actb* (ΔC_t) and converted to relative expression using the formula $2^{-\Delta C_t} \times 100$. Each bar represents the mean \pm SEM from 4 to 5 independent tissues. Labels show both the gene name and the encoded protein name with the results in male tissues shown on the left and female tissues shown on the right for each gene. Significant differences were assessed by two-way ANOVA corrected for multiple comparisons using the Tukey method ($P < .05$).

(representing roughly the middle of the standard curve for each analyte, see [Supplemental Fig. 3](#)). The intra-assay standard was 6-MP at 1200 pmoL/10 μ L. For multiple consecutive runs, only one set of interassay and intra-assay standards was done for the collective runs. The results from these 2 types of standards are depicted in [Supplemental Table 3](#) along with corresponding coefficients of variation. Coefficients of variation were all less than 15%, similar to that found previously using a similar method ([Oliveira et al, 2004](#)). The limit of detection was 49, 150, 480, and 4500 pmoL for 6-TG, 6-TU, 6-MP, and 6-MMP, respectively. These limits of detection were slightly higher than those published by Oliveira and colleagues ([Oliveira et al, 2004](#)), from which this method was designed, but sufficient for the tissue metabolite levels found in the present study.

3. Results

3.1. Gross morphology and expression of genes involved in 6-MP metabolism

The *slc43a3*-null mice were viable. No breeding abnormalities were observed when the heterozygous mice were mated. Homozygous *slc43a3*-null mice also bred successfully, but the offspring were observed to be infertile. The litter frequency and size from heterozygous pairings were typical of this mouse strain (<https://www.informatics.jax.org/silverbook/>). There were no differences in the male/female ratios, and Mendelian genetics were observed with respect to a number of KO, WT, and heterozygote offspring. Likewise, the total body weight ([Supplemental Fig. 4A](#)) and organ weights ([Supplemental Fig. 4B](#)) of the KO mice were similar to those of the WT mice, with female mice having significantly lower body and organ weights (with the exception of spleen) than the male mice. Spleen wet weight was similar (~80 mg) in male and female mice for both the WT and KO genotypes. qPCR confirmed the loss of *slc43a3* transcript in the KO mice ([Fig. 2A](#)). In WT mice, *slc43a3* showed the highest level of expression in the lung, followed by heart (4-fold lower), and then liver, kidney, duodenum, jejunum, and ileum ([Fig. 2B](#)). This is similar to what was shown in a subset of these data previously published by our laboratory ([Kim et al, 2024](#)). That previous study also showed that *slc43a3* is expressed at negligible levels in mouse brains. In all cases, there was no significant difference in *slc43a3* expression between male and female mice nor were there any significant differences between WT and KO mice in any of the tissues for any of the other genes tested ([Figs. 3 and 4](#)). There was, however, a significant sex-related difference in the expression of *slc23a4*. *Slc23a4*, which encodes for SNBT1, was significantly higher in all female tissues relative to male tissues ([Fig. 3](#)). This analysis also revealed significant tissue differences in the expression of some of the genes examined. *Slc23a4* was expressed predominantly in GI tissues. For *slc29a1* (ENT1), expression in liver > heart, lungs > kidney > GI tissues. In contrast, *slc29a2* (ENT2) was most highly expressed in the heart and kidney, followed by lungs, and then lowest in the liver and the GI tissues. With respect to the efflux pumps that have been proposed to transport 6-MP metabolites ([Wielinga et al, 2002](#)), *abcc4* (multidrug resistance-associated protein 4) expression pattern was kidney > heart, lungs >> liver and GI tissues, whereas the expression of *abcc5* (multidrug resistance-associated protein 5) was similar in all tissues examined. *Hprt*, one

Significant differences between tissue types are shown for the male data only (identical statistical differences were obtained when comparing female tissues), where bars with different letters are significantly different from each other. Significant differences between expression in male versus female tissue for each gene are shown in the female data set by “†.” There were no significant differences between WT and KO tissues for any of the genes assessed.



Fig. 4. Expression of genes in WT and KO mice encoding for enzymes involved in the metabolism of endogenous nucleobases and 6-MP. Transcript levels were determined by qPCR relative to the geometric mean of *gapdh* and *actb* (ΔCt) and converted to relative expression using the formula $2^{-\Delta Ct} \times 100$. Each bar represents the mean \pm SEM from 4 to 5 independent tissues. Labels show both the *gene* name and the encoded protein name with the results in male tissues shown on the left and female tissues shown on the right for each gene. Significant differences were assessed by two-way ANOVA corrected for multiple comparisons using the Tukey method ($P < .05$). Significant differences between tissue types are shown for the male data only (identical statistical differences were obtained when comparing female tissues), where bars with different letters are significantly different from each other. Significant differences between expression in male versus female tissue for each gene are shown in the female data set by “f.” There were no significant differences between WT and KO tissues for any of the genes assessed.

of the first enzymes in the 6-MP metabolism pathway, was expressed similarly across most of the tissues examined, but there was a slight, but significant, lower expression in the duodenum. *Aprt*, on the other hand, had the highest expression in GI tissues, followed by lungs, kidneys, and liver, and significantly lower expression yet in the heart. *Tpmt*, encoding an enzyme involved in the methylation and deactivation of 6-MP, was most highly expressed in the liver and kidney. *Xdh*, encoding an enzyme that also deactivates 6-MP, was most highly expressed in lungs, liver, duodenum, and jejunum, with significantly lower levels found in the heart and kidneys. *Prps1* and *gmps* both had significantly lower expression in the GI tissues compared with the other tissues examined. *Impdh1* was most highly expressed in the lungs, followed by the heart, and then at similarly lower levels in the other tissues examined. *Itpa* was expressed at similar levels across all tissues examined.

3.2. Pharmacokinetic analysis of 6-MP absorption and distribution

Time profiles showing the amount of 6-MP in blood 30, 90, 180, and 270 minutes following oral administration are shown in Fig. 5A. In WT mice, blood levels peaked by 90 minutes (males: 668 ± 36

pmol/ μ L; females: 993 ± 74 pmol/ μ L). In comparison, the KO mice displayed significantly lower blood levels of 6-MP at all time points. To obtain additional information on the basis for this reduction, 6-MP in the feces collected from the GI tract upon tissue processing was assessed. In both male and female mice, there was significantly more 6-MP remaining in the feces in the KO mice relative to the WT mice (Fig. 5B). Nonlinear mixed-effect population-based pharmacokinetic modeling of 6-MP blood-time profiles were performed with the stochastic approximation expectation-maximization algorithm in Monolix 2024R1 (Lixoft SAS, a Simulations Plus company, Batiment D). Extravascular administration was modeled using zero- or first-order (with or without lag time) absorption or double absorption (simultaneous first- and zero-order). 6-MP concentration-time distribution profiles were fitted to 1- or 2-compartmental models with linear elimination from the central compartment. Proportional residual error models with log-normal distributions were utilized to find the error estimates. The best structural model was selected based on the following criteria: (1) corrected Bayesian information criteria [preferred for small datasets such as this (Brewer et al, 2016)], (2) graphical assessments of goodness-of-fit plots and prediction-corrected visual predictive

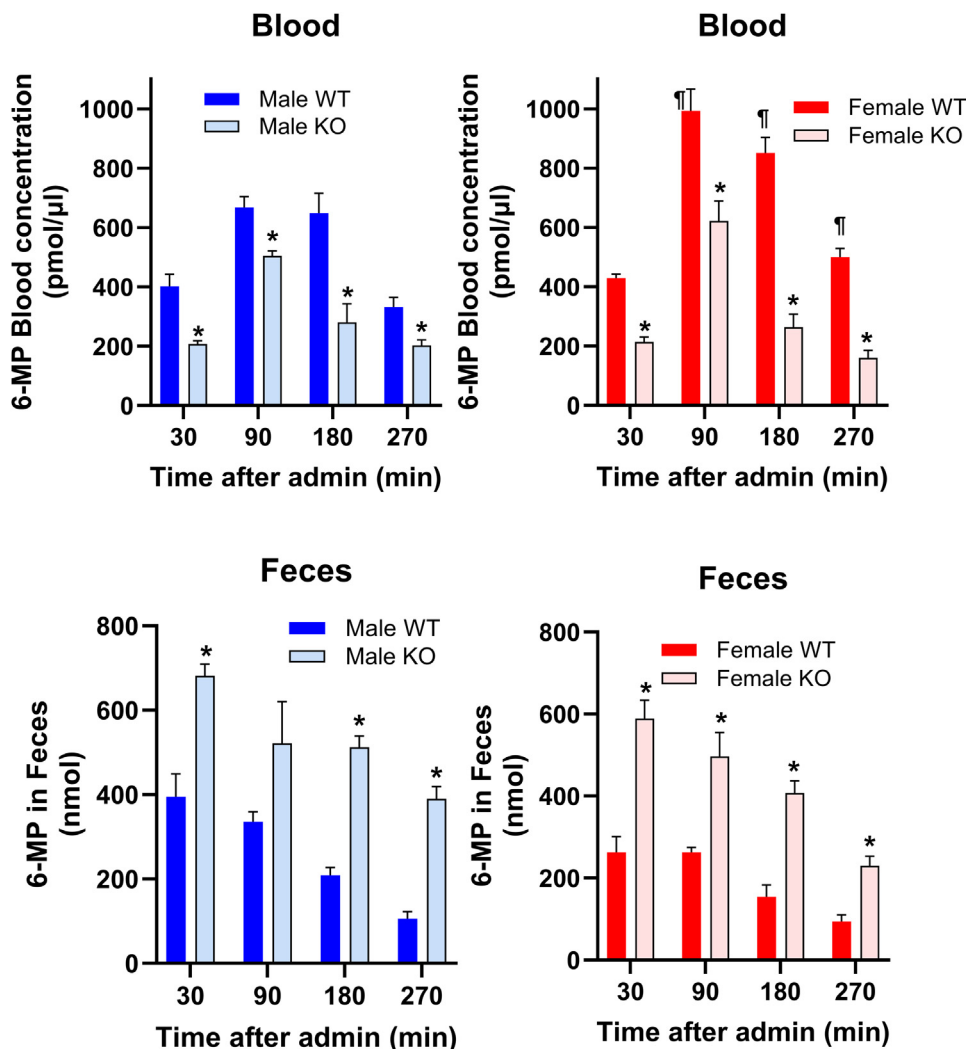


Fig. 5. 6-MP levels in blood and feces of male and female WT and KO mice. Mice were administered 75 mg/kg of 6-MP by oral gavage, and then blood was obtained by cardiac puncture and feces were obtained from the GI tract, 30-, 90-, 180- and 270-minute following administration and assessed for 6-MP levels by HPCL. Each bar represents the mean \pm SEM from 5 mice. Differences between WT and KO mice were assessed for each time point using multiple unpaired t-tests corrected for multiple comparisons using the Holm-Sidak method ($P < .05$). A significant difference between WT and KO mice is indicated with an asterisk, and a significant difference between male and female WT mice is indicated by "¶."

checks, and (3) numerical assessments of relative standard error values associated with fixed and random effects parameters. The pharmacokinetic parameters, k_a (first-order rate constant), Tk_0 (zero-order rate constant), V (apparent volume of distribution), and k (elimination rate constant) from these fits, were derived using the Bootstrap resampling module in the Monolix software package. This is a method to assess parameter uncertainty, as an alternative to calculating standard errors via inversion of the Fisher Information Matrix, particularly with sparse data sets that can lead to numerical errors in matrix inversion or biases in results caused by incorrect assumptions of asymptotic normality for parameter estimates. Pharmacokinetic parameter estimates from Bootstrap analyses for all datasets are shown in Supplemental Table 4. Based on these criteria, the concentration-time profiles for the WT mice fit best to a first-order absorption, 1-compartment model. Although the KO mice profiles fit best to a zero-order absorption, 1 compartment model (Fig. 6A). There was no significant difference between male and female WT mice in either the k_a or k parameters, but there was a significant decrease in V in the female WT mice relative to males. With respect to the KO mice, Tk_0 and k were higher in the female mice relative to males, whereas V was lower in the female mice. The shift from first-order to zero-order absorption

of 6-MP upon loss of *slc43a3* implied that ENBT1 influenced the first-order absorption component. In an attempt to show this more clearly, we subsequently modeled all the data using a double absorption (simultaneous first-order and zero-order) model. This model is the one that is best supported by past studies on 6-MP pharmacokinetics (Ding and Benet, 1979; Hawwa et al, 2008; Arun et al, 2024). The results of these analyses are provided in Fig. 6B and Supplemental Table 4 and show that the loss of *slc43a3* almost eliminated the first-order absorption component and also slightly reduced the zero-order component. The elimination constant, k , was not impacted.

3.3. AZA versus 6-MP

AZA, a prodrug to 6-MP, was administered orally to the mice at a dose (156 mg/kg) that would generate an amount of 6-MP similar to that obtained using 75 mg/kg 6-MP itself. Blood and feces levels of 6-MP as well as its tissue distribution after AZA administration were compared with that of 6-MP administration at the 90-minute time point (after administration; Table 1). The KO mice showed a decrease in 6-MP levels in the blood after AZA administration, similar to that seen with 6-MP administration, but in this case, only

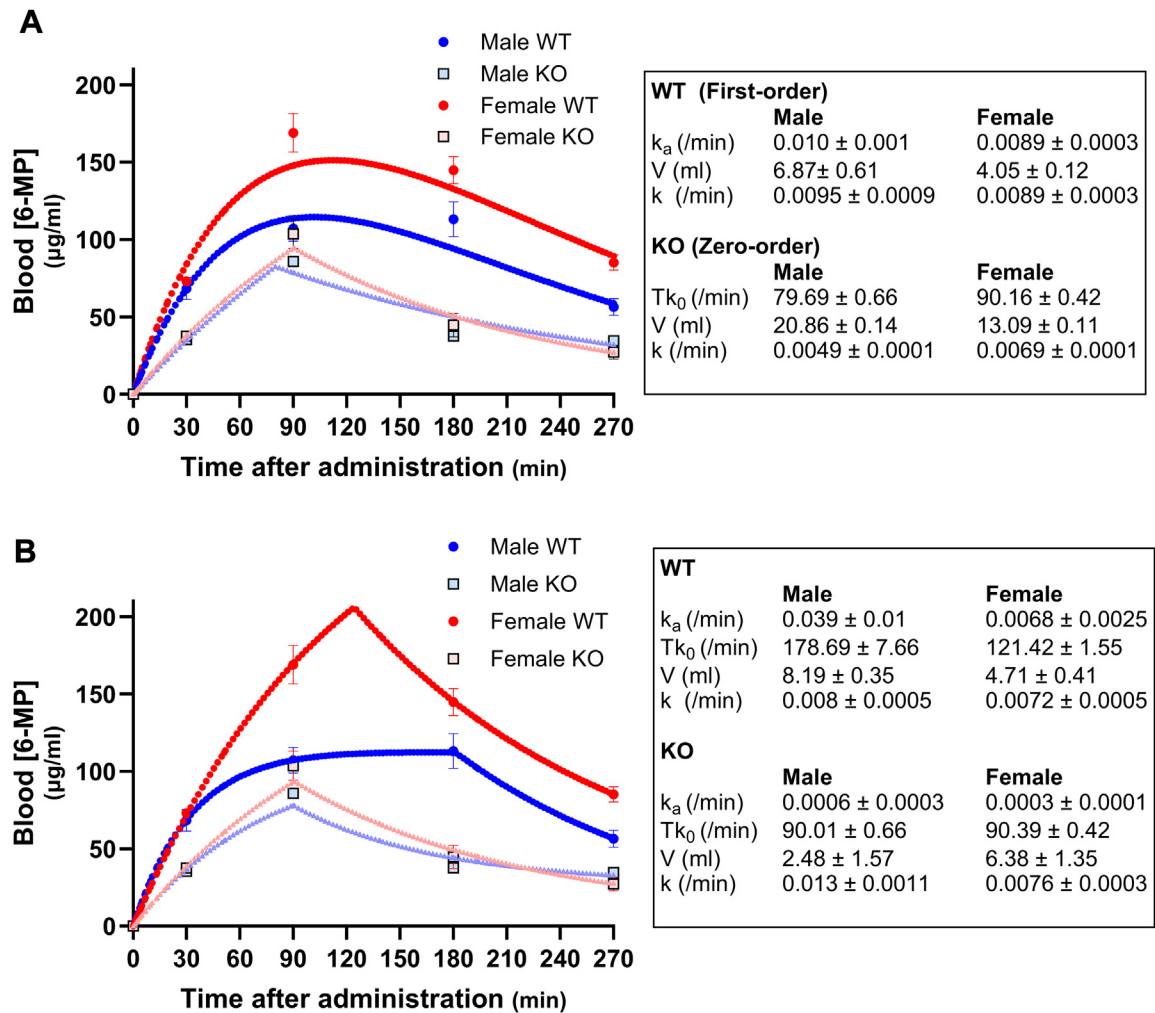


Fig. 6. Population-based pharmacokinetic modeling of 6-MP. Mice were administered 75 mg/kg of 6-MP orally and blood collected after 30, 90, 180, and 270 minutes. Each point represents the mean \pm SEM from 5 mice. The fitted line describes the predicted continuous data derived from the pharmacokinetic modeling software Monolix Suite 2024R1 assuming a single compartment with linear elimination, and A. first-order absorption for the WT mice, and zero-order absorption for the KO mice (best-fit models), B. double absorption (simultaneous zero-order and first-order absorption). The parameters derived from these pharmacokinetic models are shown to the right of each respective panel.

Table 1

Blood, feces, and tissue distribution of 6-MP 90 minutes after oral administration of 156 mg/kg AZA or 75 mg/kg 6-MP in WT and KO male and female mice

Male	AZA Administration		6-MP Administration	
	WT	KO	WT	KO
Blood (pmol/ μ L)	807 \pm 86 ^a	584 \pm 41	668 \pm 36	505 \pm 16*
Feces (nmol)	270 \pm 53	301 \pm 31	336 \pm 23	522 \pm 98
Tissues (pmol/mg)				
Heart	1736 \pm 92	1377 \pm 85	1832 \pm 115	1219 \pm 85*
Lungs	1640 \pm 96	1526 \pm 91	1875 \pm 102	1400 \pm 68*
Liver	393 \pm 20	329 \pm 26	409 \pm 24	264 \pm 16*
Kidney	749 \pm 27	503 \pm 32*	750 \pm 20	557 \pm 44*
Spleen	1074 \pm 40	746 \pm 49*	1405 \pm 133	875 \pm 75*
Duodenum	1033 \pm 74	1039 \pm 100	894 \pm 65	651 \pm 26*
Jejunum	382 \pm 22	511 \pm 60	371 \pm 15	389 \pm 35
Ileum	1738 \pm 187	2264 \pm 173	1569 \pm 88	1059 \pm 36*
Female	AZA Administration		6-MP Administration	
	WT	KO	WT	KO
Blood (pmol/ μ L)	678 \pm 52	341 \pm 27*	993 \pm 74	622 \pm 67*
Feces (nmol)	256 \pm 42	223 \pm 67	263 \pm 11	497 \pm 58*
Tissues (pmol/mg)				
Heart	1203 \pm 60	918 \pm 84	1643 \pm 88	1067 \pm 32*
Lungs	1270 \pm 69	796 \pm 42*	1905 \pm 70	1118 \pm 63*
Liver	265 \pm 3	170 \pm 7*	398 \pm 21	232 \pm 10*
Kidney	560 \pm 32	341 \pm 21*	750 \pm 40	405 \pm 20*
Spleen	870 \pm 44	478 \pm 13*	1131 \pm 56	581 \pm 29*
Duodenum	1017 \pm 179	1008 \pm 59	961 \pm 93	507 \pm 39*
Jejunum	438 \pm 24	420 \pm 31	403 \pm 15	292 \pm 9*
Ileum	1494 \pm 65	2025 \pm 125	2126 \pm 148	1014 \pm 66*

*Indicates a significant difference between WT and KO mice (two-way ANOVA corrected for multiple comparisons using the Tukey method, $P < .05$).^aEach value is the mean \pm SEM from 5 mice.

the female WT versus KO difference was statistically significant. The amount of 6-MP detected in the feces of WT mice after AZA administration was similar to that seen with 6-MP administration. However, in contrast to that seen with the administration of 6-MP, the loss of *slc43a3* in the KO mice had no effect on the amount of 6-MP in the feces after AZA administration. The distribution of 6-MP to other tissues was also examined 90 minutes after either AZA or 6-MP administration. With 6-MP administration, the loss of *slc43a3* significantly reduced the amount of 6-MP in the tissues from both male and female mice assessed 90 minutes after administration, with the exception of the jejunum in male mice. In contrast, after AZA administration, loss of *slc43a3* significantly reduced the amount of 6-MP in only the spleen and kidneys of male mice, and in the lung, liver, kidney, and spleen of female mice. Furthermore, there was a significant increase in the amount of 6-MP found in the ileum of female KO mice, compared with WT mice, and a trend in that direction in the jejunum and ileum of male mice.

3.4. Tissue distribution of 6-MP and metabolites over time

Figure 7 shows the tissue distribution of 6-MP over the full range of time points assessed. To further determine how the loss of *slc43a3* affects the distribution of 6-MP to peripheral tissues, these data were combined with those shown in Fig. 5A to calculate tissue:blood ratios for lung, heart, liver, kidney, spleen, and the GI tissues duodenum, jejunum, and ileum after 6-MP administration for 30, 90, 180, and 270 minutes (Fig. 8). In both male and female mice, the loss of *slc43a3* led to a significant reduction in the tissue:blood ratio of 6-MP in all tissues examined 30 minutes after administration, except for liver and jejunum. This difference was gone by 90 minutes after administration. However, when assessed 270 minutes after 6-MP administration, the KO mice had significantly higher tissue:blood ratios in all of the GI tissues examined (duodenum, jejunum, and ileum) relative to that seen in WT mice.

The female KO mice also had significantly increased tissue:blood ratios in the heart and lungs at this later time point.

In parallel with the measurement of 6-MP (Fig. 7), we assessed the levels of 6-TU, 6-MMP, and 6-TGN (detected after hydrolysis as 6-TG by HPLC) in blood, feces, and the GI tissues duodenum, jejunum, and ileum (Fig. 9) as well as peripheral tissues such as liver, heart, lung, spleen, and kidneys (Fig. 10) to determine if loss of *slc43a3* modified the in vivo metabolism of 6-MP. Brain tissue was also analyzed for 6-MP and metabolite levels, but the concentrations were consistently below the level of detection.

Focusing on the WT mice, of the 3 metabolites assessed, 6-MMP was found at the highest levels in all tissues, followed by 6-TU, and then 6-TGN. When assessed at the 90-minute time point after 6-MP administration, the lungs and spleen had the highest concentrations of all metabolites, followed by the heart, then the kidney, and the liver. When aggregating the levels of 6-MP and its metabolites, it was calculated that about 70% of the original dose of 6-MP was recovered through this HPLC analysis. The remainder was likely lost in urine or distributed to other tissues not assessed in this study. The impact of the loss of *slc43a3* on metabolite profiles varied among the tissues, detailed as follows.

3.5. Small intestine

In the duodenum, jejunum, and ileum, all 3 metabolites peaked at the 180-minute time point in both male and female WT mice, with ileum showing the highest concentrations of 6-MP and its metabolites. KO mouse tissues, on the other hand, increased in their levels of all 3 metabolites across all the time points. The metabolites were found to be consistently lower in the KO mouse intestine compared with that from WT mice up to 180 minutes. As seen for 6-MP, although, by 270 minutes the concentrations of all 3 6-MP metabolites in the KO mouse GI tissues were significantly higher than those detected in the WT mouse.

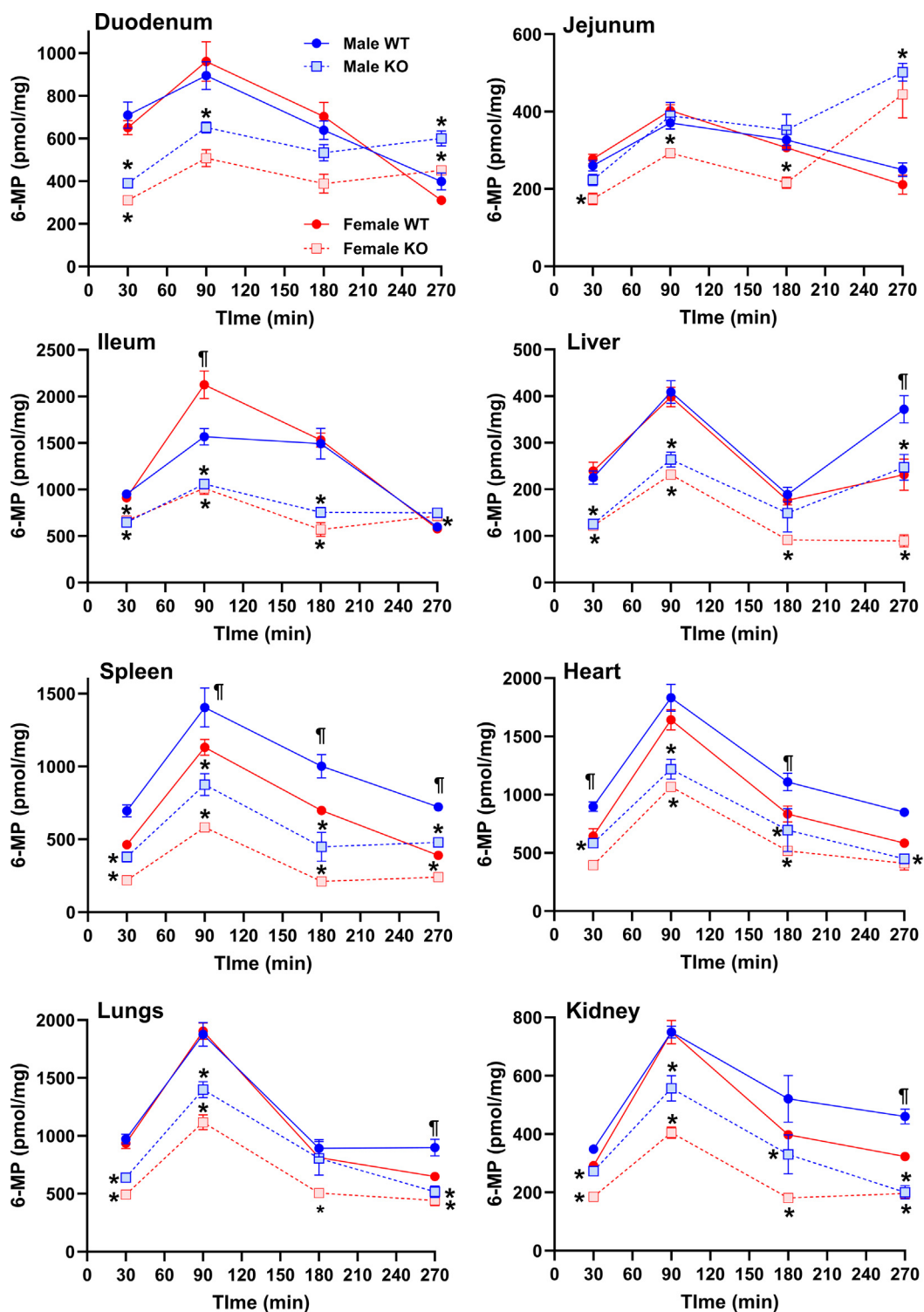


Fig. 7. Time course of tissue distribution of orally administered 6-MP. Mice were administered 75 mg/kg 6-MP by oral gavage. The duodenum, jejunum, ileum, liver, spleen, heart, lungs, and kidney were removed 30, 90, 180, or 270 minutes after administration and assessed for 6-MP levels by HPLC. Each point represents the mean \pm SEM derived from 5 mice. Differences between WT and KO mice were assessed using two-way ANOVA corrected for multiple comparisons by the Tukey method ($P < .05$). A significant difference between WT and KO mice is indicated with an asterisk, and a significant difference between male and female WT mice is indicated by “#.”

3.6. Blood

The blood concentrations of all 3 6-MP metabolites increased with time up to 270 minutes, with significantly lower levels seen in the KO mice relative to WT mice. There was also a clear sex difference in 6-MMP levels in the WT mice with females having higher levels than males. This difference was not seen in the KO mice.

3.7. Liver

The liver is the first tissue that orally administered 6-MP is distributed to after the GI tract. 6-MP itself was found at significantly lower levels in the liver from KO mice relative to those from WT mice. There was generally no difference in 6-MMP or 6-TGN levels in the liver from WT and KO mice, except for significantly

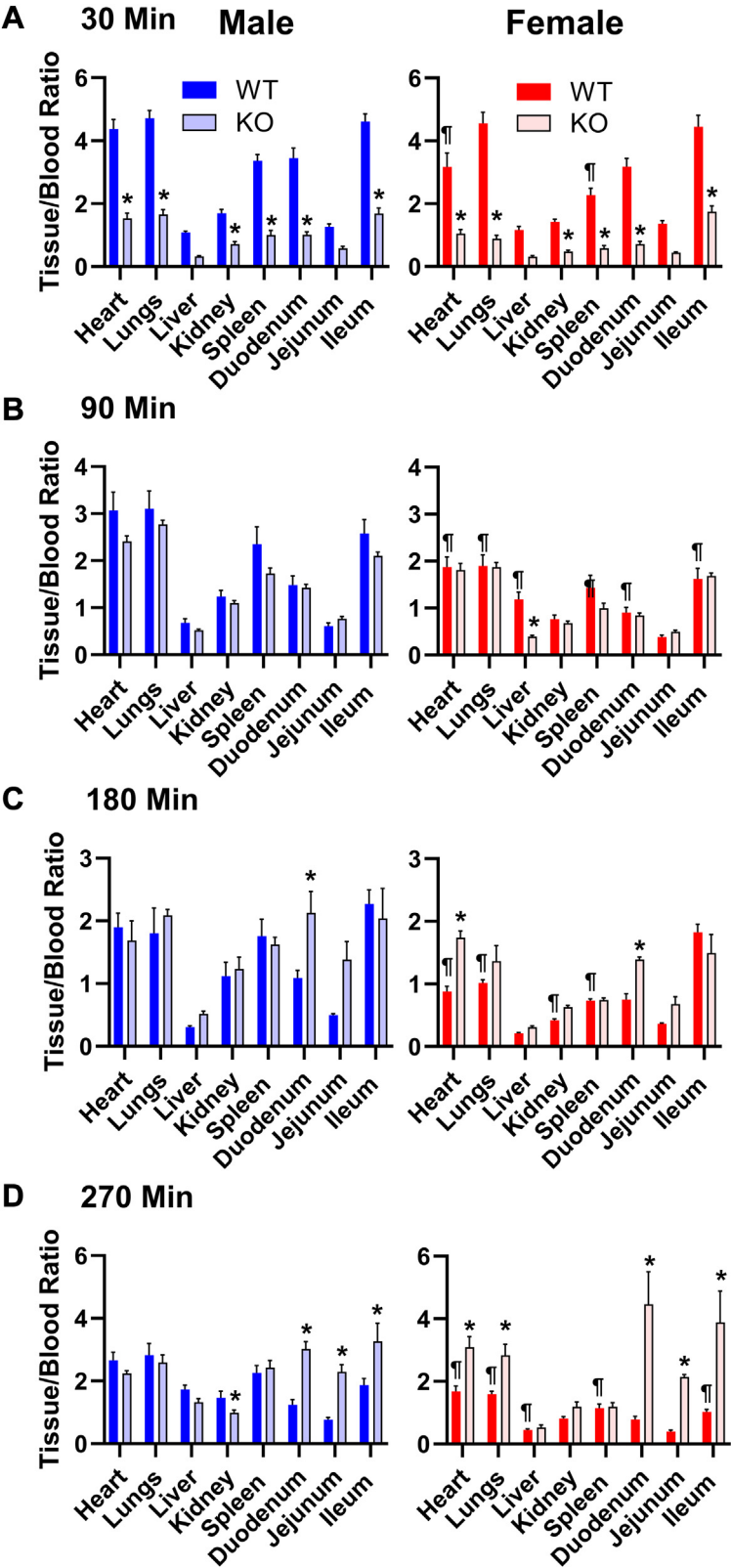


Fig. 8. 6-MP tissue:blood ratios. Mice were administered 75 mg/kg 6-MP by oral gavage. Blood was collected by cardiac puncture and various organs were removed 30 (A), 90 (B), 180 (C), and 270 (D) minutes after administration. The concentration of 6-MP in each organ was divided by the blood concentration of 6-MP for each time point. Bars represent the mean \pm SEM derived from 5 mice. Differences between WT and KO mice were assessed using two-way ANOVA corrected for multiple comparisons by the Tukey method ($P < .05$). A significant difference between WT and KO mice is indicated with an asterisk, and a significant difference between male and female WT mice is indicated by “¶.”

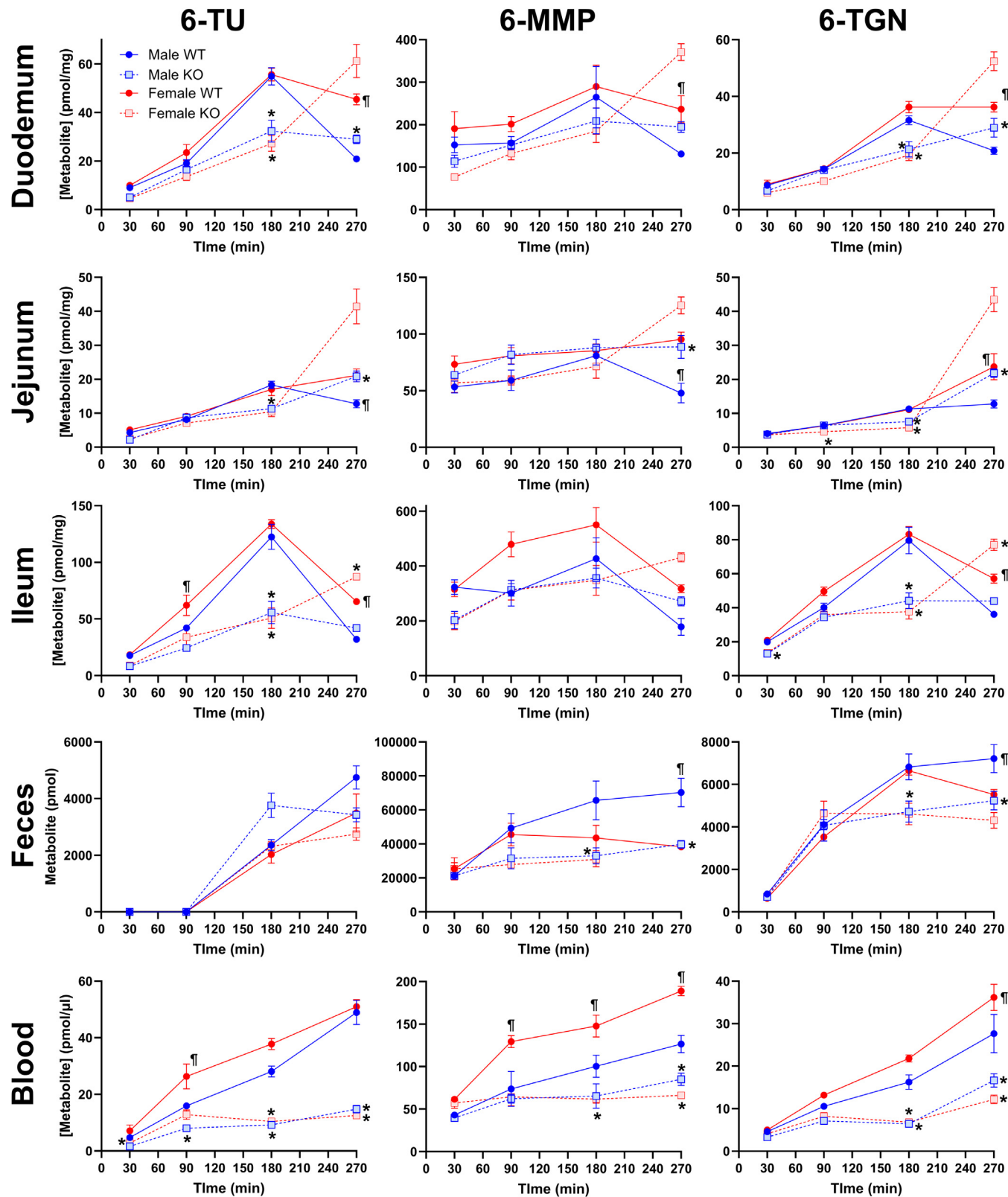


Fig. 9. Distribution of 6-MP metabolites in GI tissues and blood. Mice were administered 75 mg/kg 6-MP by oral gavage. Duodenum, jejunum, ileum, feces, and blood were collected at 30, 90, 180, or 270 minutes after administration and assessed for 6-TU, 6-MMP, and 6-TGN levels by HPLC. Each point represents the mean \pm SEM derived from 5 mice. Differences between WT and KO mice were assessed using two-way ANOVA corrected for multiple comparisons by the Tukey method ($P < .05$). A significant difference between WT and KO mice is indicated with an asterisk, and a significant difference between male and female WT mice is indicated by “¶.”

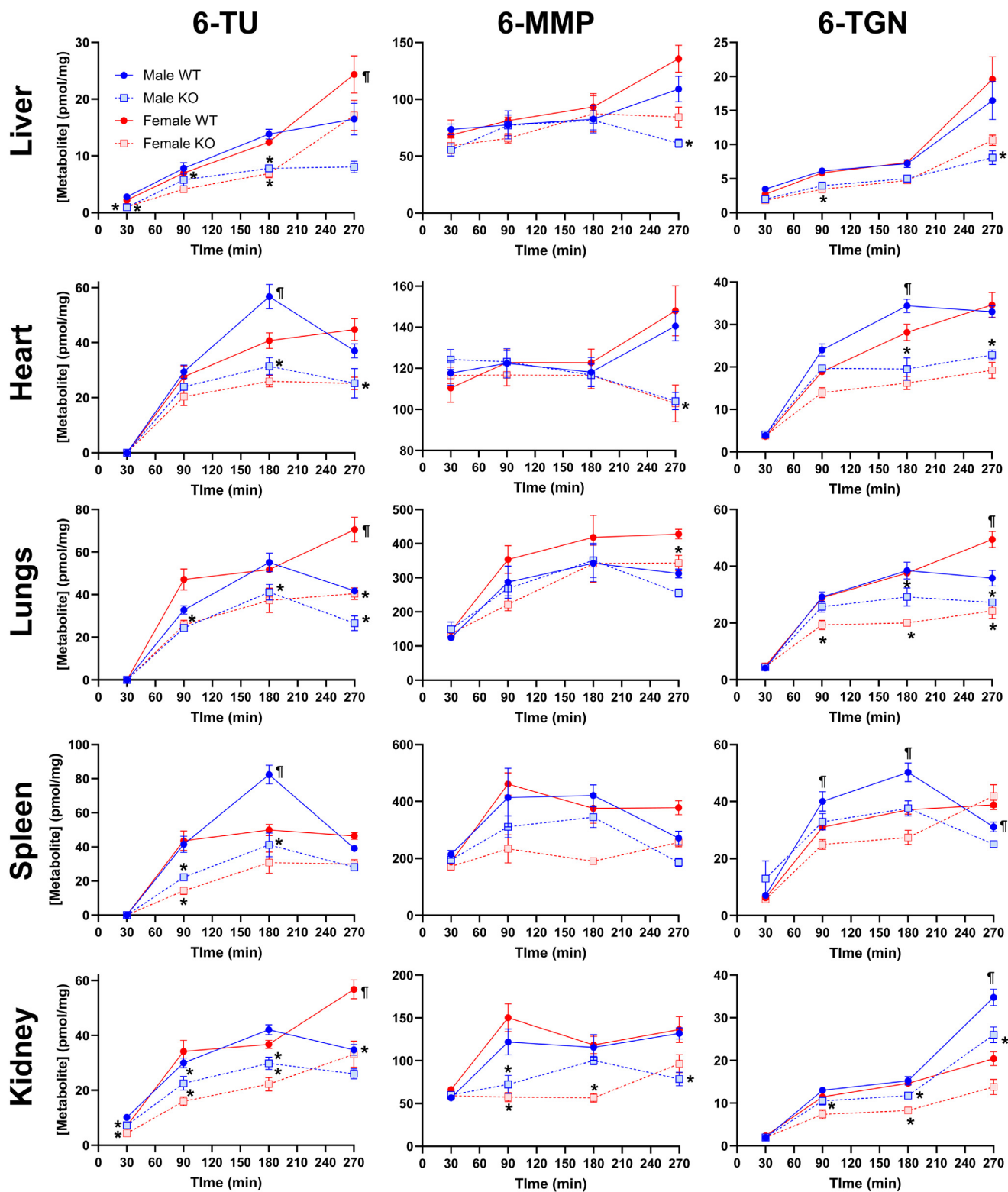


Fig. 10. Distribution of 6-MP metabolites in peripheral tissues. Mice were administered 75 mg/kg 6-MP by oral gavage. Liver, heart, lungs, spleen, and kidneys were collected at 30, 90, 180, or 270 minutes after administration and assessed for 6-TU, 6-MMP, and 6-TGN levels by HPLC. Each point represents the mean \pm SEM derived from 5 mice. Differences between WT and KO mice were assessed using two-way ANOVA corrected for multiple comparisons by the Tukey method ($P < .05$). A significant difference between WT and KO mice is indicated with an asterisk, and a significant difference between male and female WT mice is indicated by “¶.”

lower levels of both after 270 minutes in the male KO mice. However, the levels of 6-TU in the liver from the KO mice were significantly lower than those seen in the WT mice across all time points.

3.8. Heart and lungs

These highly perfused tissues tended to show a similar profile of 6-MP metabolites over time. 6-MMP was the first metabolite

detected after administration, with 6-TU and 6-TGN only appearing in significant concentrations 90 minutes after administration. In terms of WT versus KO mice, 6-MMP levels were lower in the KO tissues only in the female mice at the 270-minute time point. In contrast, 6-TGN levels were similar in female KO and WT heart tissues, but hearts from male KO mice had significantly lower levels of 6-TGN. Lungs, on the other hand, had decreased 6-TGN levels at longer time points in both the female and male KO mice compared with the WT mice. 6-TU was also found at lower levels in the heart and lungs of KO mice, but this difference was only significant at the longer time points.

3.9. Spleen

The spleen from KO mice had significantly lower 6-MP levels than the WT mice over all the time points examined. There was no significant difference in 6-MMP or 6-TGN levels between WT and KO spleen. Male KO mice had significantly lower levels of 6-TU in the spleen relative to WT mice at the 90- and 180-minute time points, whereas spleens from female KO mice only showed a decrease in 6-TU levels relative to WT mice at the 270-minute time point.

3.10. Kidneys

Kidneys from the KO mice generally showed a lower content of both 6-MMP and 6-MP, with the difference being most significant at the 90-minute time point after 6-MP administration. Only the male KO mice, however, showed a consistent decrease in 6-TGN levels in the kidney relative to WT mice. 6-TU showed the greatest difference between WT and KO mice, with the kidneys from both male and female KO mice having significantly lower levels across all 3 of the later time points.

4. Discussion

We established a novel *slc43a3*-null mouse model that can be used to assess the role of ENBT1 in drug actions and the physiological handling of purine nucleobases. The mice were viable and reproduced successfully via heterozygote pairings with no obvious developmental or morphological consequences, at least up to the age of 12 weeks (the maximum age at which the mice were used in this study). Furthermore, there are no confounding compensatory changes in the *slc43a3*-null mice with respect to other transporters and enzymes involved in nucleobase or nucleobase analog metabolism. This does not preclude there being more subtle changes in physiological function in the *slc43a3*-null mice that may be revealed upon further investigation. Indeed, given the role of purine nucleobases and nucleosides in cellular regulation and energy metabolism (Huang et al, 2021), it would be surprising if there was not some disruption.

Our focus, however, was on the role of ENBT1 in the bio-distribution of the therapeutic nucleobase analog 6-MP. The loss of *slc43a3*-encoded ENBT1 clearly led to a dramatic decrease in the blood levels of 6-MP after oral administration, suggesting that this transporter contributes significantly to the absorption of 6-MP from the GI tract. This is corroborated by the concurrent increase in 6-MP found in the gut lumen (feces) in the KO mice. Population-based pharmacokinetic modeling of the 6-MP blood concentration-time profiles highlighted a loss of first-order absorption of 6-MP in the KO mice leaving only a zero-order process mediating the reduced absorption of 6-MP. This suggests that ENBT1 is a major contributor to the first-order component of 6-MP absorption in mice.

Facilitated diffusion solute transporters, like ENBT1, are typically located on the basolateral membrane of polarized cells such as gut endothelial cells where they mediate the flux of substrates from the intracellular compartment to the blood (Oswald, 2022). Although this has not been confirmed for ENBT1 in gut endothelium, it has been shown that ENBT1 is trafficked to the basolateral membrane of hepatic cell lines (Takenaka et al, 2020). Working in tandem with the basolateral equilibrative transporter is typically a concentrative transport system located on the apical membrane of the cells. In the case of nucleobase transport in mice, this apical transporter is likely SNBT1. SNBT1 is expressed at high levels in the intestines as shown in the current study and by others (Yamamoto et al, 2010). Humans, however, do not express SNBT1 and must employ an, as yet unidentified, different transport process to mediate the apical cellular uptake of nucleobases.

With the loss of ENBT1 in the KO mice, SNBT1 would deliver 6-MP into the cells from the gut lumen, but the exit of the drug to the blood would be dependent on passive diffusion or other transporters such as ENT1 and ENT2 that have much lower affinity than ENBT1 for 6-MP (Nagai et al, 2007; Yao et al, 2011). This may lead to an accumulation of 6-MP and its metabolites intracellularly in the enteric cells. We show that transcripts for the enzymes involved in 6-MP metabolism (XDH, TPMT, hypoxanthine-guanine phosphoribosyltransferase, and GMPs) are highly expressed in the GI tissues. The increased level of 6-MP metabolites seen in the GI tissues of KO mice, relative to WT mice, 270 minutes after administration supports this possibility. The ileum was the segment of the small intestine that accrued the highest content of 6-MP and its metabolites per mg of tissue in both the WT and KO groups. This corroborates previous findings of Zou and colleagues who found that the ileum accumulated the highest concentrations of 6-MP after oral administration (Zou et al, 2021). This finding is also supported by a study demonstrating that the ileum has the highest expression of SNBT1 among the 3 segments of the small intestine in rodents (Yamamoto et al, 2010).

Once absorbed from the GI tract, 6-MP is exposed to the liver and further metabolized, predominantly by TPMT and XDH which are both highly expressed in the mouse liver. This would lead to the production of high levels of the metabolites 6-MMP (by TPMT) and 6-TU (by XDH). We do observe that the major metabolite of 6-MP distributed throughout the body is 6-MMP, as has been reported by others (Pelín et al, 2017). 6-TU was found at much lower levels, possibly due to its rapid elimination in urine which was not analyzed in this study. Although the livers from KO mice had lower levels of 6-TU than those of the WT mice, there was no difference between livers of WT and KO mice with respect to the amount of 6-MMP. This is in spite of the fact that livers of KO mice would receive significantly lower levels of 6-MP due to the reduced absorption from the GI tract. This may reflect the saturation of the TPMT enzyme in the liver at the concentrations of 6-MP seen in the KO mice. TPMT has been reported to have a K_m for 6-MP of about 120 μ M (Kröplin et al, 1999). The blood concentrations of 6-MP in the KO mice after first-pass metabolism were greater than 500 μ M, and blood from the WT mice had levels approaching 1 mM. The concentrations of 6-MP in the portal vein, prehepatic metabolism, would be expected to be even higher.

Slc43a3 is highly expressed in the heart and lungs, and we have previously shown ENBT1 transport activity in microvascular endothelial cells (Bone and Hammond, 2007). Therefore, it may be anticipated that the loss of ENBT1-mediated 6-MP transport would impact the tissue distribution of 6-MP, particularly in those tissues with a high expression of the transporter. This possibility is supported by the significantly lower tissue:blood ratios of 6-MP in all tissues from the KO mice relative to WT mice 30 minutes after oral administration. By 90 minutes, this difference is largely gone,

suggesting that 6-MP takes longer to distribute from blood to tissue in the KO mice but eventually achieves similar levels during the absorption phase. However, at longer times after administration, GI tissues in both male and female KO mice as well as hearts and lungs of female KO mice actually show a significantly higher concentration of 6-MP than their WT counterparts. The mechanism underlying this reversal is obscure, but it may reflect a decreased efflux of 6-MP from the tissues, due to the lack of ENBT1 (which is bidirectional; Ruel et al, 2019), after absorption is complete during the elimination phase of the distribution.

AZA is often used therapeutically instead of 6-MP for the treatment of IBD due to its better absorption characteristics. AZA has a LogP value of 1.17 compared with that of 6-MP with a LogP of -0.19 (Knox et al, 2024), giving AZA an enhanced ability to passively diffuse across membranes. AZA is metabolized to 6-MP via glutathione transferase, mainly in the liver but also to some extent in the GI tract (Modén and Mannervik, 2014). We have shown that AZA does not interact directly with ENBT1, and, therefore, the absorption of AZA would not be expected to be impacted to the same degree by the loss of ENBT1. We tested this hypothesis by comparing the levels of 6-MP and its metabolites in blood and tissues after administration of an amount of AZA (156 mg/kg) that would generate a similar amount of 6-MP as that achieved with the administration of 75 mg/kg 6-MP orally. The accumulation of 6-MP and its metabolites showed no significant differences within the GI tissues between WT and KO after the administration of AZA. However, similar to that seen with 6-MP administration, 6-MP and its metabolites generated after AZA administration was consistently higher in WT compared with KO in organs that express the highest levels of *slc43a3* including the heart and lungs. The blood levels of 6-MP in the WT mice were also significantly higher after AZA administration relative to that seen with 6-MP administration, indicating enhanced bioavailability, likely due to decreased loss of 6-MP due to metabolism in the GI tract. This suggests that the absence of ENBT1 affects the tissue uptake of the 6-MP generated from AZA postabsorption, but the absence of ENBT1 does not impact the absorption of AZA from the lumen. This further emphasizes the important role of ENBT1 in the absorption and distribution of 6-MP.

Finally, it is worth noting the significant male/female differences observed in this study in the absorption and metabolism of 6-MP. Blood levels of 6-MP in female WT mice after oral administration at a dose of 75 mg/kg were significantly higher than those achieved in male WT mice at 90- and 180-minute postadministration. This may be due to the increased expression of *slc23a4* that was noted in female mice, leading to enhanced absorption of 6-MP via *slc43a3*-encoded SNBT1 in the female mice.

5. Summary

We have established that C57BL/6 mice with a global deletion of *slc43a3* are viable with no gross morphological abnormalities. Using this model, we have shown that the loss of *slc43a3* in these mice significantly reduces the absorption and tissue distribution of 6-MP, presumably due to the loss of the encoded transporter ENBT1 in the GI tract and other tissues including heart and lungs. These data suggest that variability in human expression of *SLC43A3* could be a factor in the variability in plasma 6-MP levels and therapeutic response to 6-MP and its prodrug AZA when used in the treatment of ALL and IBD. Although the extent of variability in the expression of *SLC43A3* in the human population has not been defined to date, our laboratory has preliminary data showing that lymphoblasts from pediatric ALL patients ($n = 40$) vary by more than 20-fold in their expression of *SLC43A3* (Ruel, 2024). In addition, over 585 protein variants of ENBT1 (UniProt ID Q8NBI5; Consortium, 2024)

have been documented but their functionality and allele frequency in human populations have not been defined. Further research on the pharmacogenomics of *SLC43A3* is clearly warranted.

Abbreviations

6-MMP, 6-methylmercaptopurine; 6-MP, 6-mercaptopurine; 6-TGN, 6-thioguanine nucleotides; 6-TU, 6-thiourate; AZA, azathioprine; ENBT1, equilibrative nucleobase transporter 1; ENT1, equilibrative nucleoside transporter 1; ENT2, equilibrative nucleoside transporter 2; GI, gastrointestinal; GMPS, guanosine monophosphate synthetase; HPLC, high-performance liquid chromatography; HPRT, hypoxanthine-guanine phosphoribosyltransferase; KO, knockout; SNBT1, sodium-dependent nucleobase transporter 1; TPMT, thio-purine methyl transferase; WT, wild-type; XDH, xanthine dehydrogenase.

Acknowledgments

The HPLC analyses were conducted in the Faculty of Medicine and Dentistry Lipodomics Core Research Facility with expert technical assistance provided by facility coordinator, Audric Moses. We also wish to thank Tony Kiang (Faculty of Pharmacy and Pharmaceutical Sciences) for advice regarding the design of the HPLC analysis and for recommending and advising on the appropriate use of the Monolix PK software package. We also extend our appreciation to our laboratory assistant Tierah Hinchliffe for the maintenance of the mouse colony and assistance with laboratory management. ALS acknowledges support of the Alberta Provincial Government by way of an Alberta Graduate Excellence Scholarship award. This work was supported by funding provided to J.R.H. by the Canadian Institute of Health Research under Grant #168913.

Financial support

This work was supported by funding provided to J.R.H. by the Canadian Institutes of Health Research under Grant #168913. This study was conducted as part of the graduate thesis work of Aaron L. Sayler.

Conflict of interest

No author has an actual or perceived conflict of interest with the contents of this article.

Data availability

All experimental data are included in this manuscript.

Authorship contributions

Participated in research design: Sayler, Hammond.

Conducted experiments: Sayler, Dean.

Performed data analysis: Sayler, Dean, Hammond.

Wrote or contributed to writing of the manuscript: Sayler, Hammond.

Supplemental material

This article has supplemental material available at dmd.aspetjournals.org.

References

- Abaji R and Kraljic M (2017) Thiopurine S-methyltransferase polymorphisms in acute lymphoblastic leukemia, inflammatory bowel disease and autoimmune disorders: influence on treatment response. *Pharmacogenomics Pers Med* **10**: 143–156.
- Adam de Beaumais T, Medard Y, Amblard O, Goldwirth L, Simonin M, Martinez Vinson C, Petit A, and Jacqz-Aigrain E (2022) Improved HPLC quantification of 6-mercaptopurine metabolites in red blood cells: monitoring data and literature analysis. *Int J Mol Sci* **23**:11885.
- Arun B, Joshi M, Kakkar AK, Madki S, Ivaturi V, Chinnaswamy G, Banavali S, and Gota V (2024) Bioequivalence study followed by model-informed dose optimization of a powder for oral suspension of 6-mercaptopurine. *Pediatr Blood Cancer* **71**:e30813.
- Barba E, Kontou PI, Michalopoulos I, Bagos PG, and Braliou GG (2022) Association of ITPA gene polymorphisms with adverse effects of AZA/6-MP administration: a systematic review and meta-analysis. *Pharmacogenomics J* **22**:39–54.
- Bone DB and Hammond JR (2007) Nucleoside and nucleobase transporters of primary human cardiac microvascular endothelial cells: characterization of a novel nucleobase transporter. *Am J Physiol Heart Circ Physiol* **293**:H3325–H3332.
- Brewer MJ, Butler A, and Cooksley SL (2016) The relative performance of AIC, AICC and BIC in the presence of unobserved heterogeneity. *Methods Ecol Evol* **7**:679–692.
- Casteleyn C, Rekecki A, Van der Aa A, Simoons P, and Van den Broeck W (2010) Surface area assessment of the murine intestinal tract as a prerequisite for oral dose translation from mouse to man. *Lab Anim* **44**:176–183.
- Consortium TU (2024) UniProt: the universal protein knowledgebase in 2025. *Nucl Acids Res* **53**:D609–D617.
- Dervieux T and Bouliere R (1998) Simultaneous determination of 6-thioguanine and methyl 6-mercaptopurine nucleotides of azathioprine in red blood cells by HPLC. *Clin Chem* **44**:551–555.
- Ding TL and Benet LZ (1979) Comparative bioavailability and pharmacokinetic studies of azathioprine and 6-mercaptopurine in the rhesus monkey. *Drug Metab Dispos* **7**:373–377.
- Du S, Huang X, He X, Mao M, Chen M, Zhang R, Shao H, Lv Z, Liu X, and Chuan J (2024) Association of NUDT15 gene polymorphism with adverse reaction, treatment efficacy, and dose of 6-mercaptopurine in patients with acute lymphoblastic leukemia: a systematic review and meta-analysis. *Haematologica* **109**:1053–1068.
- Dubinsky MC (2004) Azathioprine, 6-mercaptopurine in inflammatory bowel disease: pharmacology, efficacy, and safety. *Clinical Gastroenterology and Hepatology* **2**:731–743.
- Dutta S and Sengupta P (2016) Men and mice: relating their ages. *Life Sci* **152**: 244–248.
- Endresen L, Lie SO, Storm-Mathisen I, Rugstad HE, and Stokke O (1990) Pharmacokinetics of oral 6-mercaptopurine: relationship between plasma levels and urine excretion of parent drug. *Therapeutic Drug Monitoring* **12**:227–234.
- Estlin EJ (2001) Continuing therapy for childhood acute lymphoblastic leukaemia: clinical and cellular pharmacology of methotrexate, 6-mercaptopurine and 6-thioguanine. *Cancer Treat Rev* **27**:351–363.
- Folch J, Lees M, and Sloane Stanley GH (1957) A simple method for the isolation and purification of total lipides from animal tissues. *J Biol Chem* **226**:497–509.
- Galetin A, Brouwer KLR, Tweedie D, Yoshida K, Sjöstedt N, Aleksunes L, Chu X, Evers R, Hafey MJ, Lai Y, et al (2024) Membrane transporters in drug development and as determinants of precision medicine. *Nat Rev Drug Dis* **23**:255–280.
- Gupta S and Bhatia S (2017) Optimizing medication adherence in children with cancer. *Curr Opin Pediatr* **29**:41–45.
- Hawwa AF, Collier PS, Millership JS, McCarthy A, Dempsey S, Cairns C, and McElroy JC (2008) Population pharmacokinetic and pharmacogenetic analysis of 6-mercaptopurine in paediatric patients with acute lymphoblastic leukaemia. *Br J Clin Pharmacol* **66**:826–837.
- Huang Z, Xie N, Illes P, Di Virgilio F, Ulrich H, Semyanov A, Verkhatsky A, Sperlagh B, Yu S-G, Huang C, and Tang Y (2021) From purines to purinergic signalling: molecular functions and human diseases. *Signal Transduct Target Ther* **6**:162.
- Kato Y, Matsushita T, Chiba K, Hijiya N, Yokoyama T, and Ishizaki T (1991) Dose-dependent kinetics of orally administered 6-mercaptopurine in children with leukemia. *J Pediatr* **119**:311–316.
- Kim CS, Saylor AL, Dean H, Ruel NM, and Hammond JR (2024) Functional comparison of human and murine equilibrative nucleobase transporter 1. *PLoS One* **19**:e0311519.
- Knox C, Wilson M, Klinger CM, Franklin M, Oler E, Wilson A, Pon A, Cox J, Chin NEL, Strawbridge SA, et al (2024) DrugBank 6.0: the DrugBank knowledgebase for 2024. *Nucleic Acids Res* **52**:D1265–D1275.
- Kröplin T, Fischer C, and Iven H (1999) Inhibition of thiopurine S-methyltransferase activity by impurities in commercially available substrates: a factor for differing results of TPMT measurements. *Eur J Clin Pharmacol* **55**:285–291.
- Kurowski V and Iven H (1991) Plasma concentrations and organ distribution of thiopurines after oral application of azathioprine in mice. *Cancer Chemother Pharmacol* **28**:7–14.
- Lafolie P, Björk O, Hayder S, Åhrström L, and Peterson C (1989) Variability of 6-mercaptopurine pharmacokinetics during oral maintenance therapy of children with acute leukemia. *Med Oncol Tumor Pharmacother* **6**:259–265.
- Lonnerholm G, Kreuger A, Lindstrom B, Ludvigsson J, and Myrdal U (1986) Plasma and erythrocyte concentrations of mercaptopurine after oral administration in children. *Pediatr Hematol Oncol* **3**:27–35.
- McLeod HL, Krynetski EY, Relling MV, and Evans WE (2000) Genetic polymorphism of thiopurine methyltransferase and its clinical relevance for childhood acute lymphoblastic leukemia. *Leukemia* **14**:567–572.
- Modén O and Mannervik B (2014) Glutathione transferases in the bioactivation of azathioprine. *Adv Cancer Res* **122**:199–244.
- Nagai K, Nagasawa K, Kihara Y, Okuda H, and Fujimoto S (2007) Anticancer nucleobase analogues 6-mercaptopurine and 6-thioguanine are novel substrates for equilibrative nucleoside transporter 2. *Int J Pharm* **333**:56–61.
- Nair AB and Jacob S (2016) A simple practice guide for dose conversion between animals and human. *J Basic Clin Pharm* **7**:27–31.
- Nielsen OH, Vainer B, and Rask-Madsen J (2001) Review article: the treatment of inflammatory bowel disease with 6-mercaptopurine or azathioprine. *Aliment Pharmacol Ther* **15**:1699–1708.
- Oliveira BM, Romanha AJ, Alves TM, Viana MB, and Zani CL (2004) An improved HPLC method for the quantitation of 6-mercaptopurine and its metabolites in red blood cells. *Braz J Med Biol Res* **37**:649–658.
- Oswald S (2022) Drug transporters in the human intestine, in *Drug Transporters*, pp 333–359.
- Pelin M, Genova E, Fusco L, Marisat M, Hofmann U, Favretto D, Lucafo M, Taddio A, Martelossi S, Ventura A, et al (2017) Pharmacokinetics and pharmacodynamics of thiopurines in an in vitro model of human hepatocytes: insights from an innovative mass spectrometry assay. *Chem Biol Interact* **275**:189–195.
- Ruel NM (2024) *Function and Regulation of Equilibrative Nucleobase Transporter 1 in Acute Lymphoblastic Leukemia*. Ph.D. thesis, University of Alberta, Education and Research Archive.
- Ruel NM, Nguyen KH, Kim CS, Andrade LPS, and Hammond JR (2022) Impact of SLC43A3/ENBT1 expression and function on 6-mercaptopurine transport and cytotoxicity in human acute lymphoblastic leukemia cells. *J Pharmacol Exp Ther* **382**:335–345.
- Ruel NM, Nguyen KH, Vilas G, and Hammond JR (2019) Characterization of 6-mercaptopurine transport by the SLC43A3-encoded nucleobase transporter. *Mol Pharmacol* **95**:584–596.
- Takenaka R, Yasujima T, Furukawa J, Hishikawa Y, Yamashiro T, Ohta K, Inoue K, and Yuasa H (2020) Functional analysis of the role of equilibrative nucleobase transporter 1 (ENBT1/SLC43A3) in adenine transport in HepG2 cells. *J Pharm Sci* **109**:2622–2628.
- Toksvang LN, Lee SHR, Yang JJ, and Schmiegelow K (2022) Maintenance therapy for acute lymphoblastic leukemia: basic science and clinical translations. *Leukemia* **36**:1749–1758.
- Wieling PR, Reid G, Challa EE, van der Heijden I, van Deemter L, de Haas M, Mol C, Kuil AJ, Groeneveld E, Schuetz JD, et al (2002) Thiopurine metabolism and identification of the thiopurine metabolites transported by MRP4 and MRP5 overexpressed in human embryonic kidney cells. *Mol Pharmacol* **62**: 1321–1331.
- Yamamoto S, Inoue K, Murata T, Kamigaso S, Yasujima T, Maeda JY, Yoshida Y, Ohta KY, and Yuasa H (2010) Identification and functional characterization of the first nucleobase transporter in mammals: implication in the species difference in the intestinal absorption mechanism of nucleobases and their analogs between higher primates and other mammals. *J Biol Chem* **285**: 6522–6531.
- Yao SY, Ng AM, Cass CE, Baldwin SA, and Young JD (2011) Nucleobase transport by human equilibrative nucleoside transporter 1 (hENT1). *J Biol Chem* **286**: 32552–32562.
- Yuasa H, Yasujima T, and Inoue K (2020) Current understanding of the intestinal absorption of nucleobases and analogs. *Biol Pharm Bull* **43**:1293–1300.
- Zou Y, Mei D, Yuan J, Han J, Xu J, Sun N, He H, Yang C, and Zhao L (2021) Preparation, characterization, pharmacokinetic, and therapeutic potential of novel 6-mercaptopurine-loaded oral nanomedicines for acute lymphoblastic leukemia. *Int J Nanomedicine* **16**:1127–1141.